J|A|C|S ARTICLES

Published on Web 07/28/2010

Unraveling the Electron Spin Resonance Pattern of Nonsymmetric Radicals with 30 Fluorine Atoms: Electron Spin Resonance and Vis−Near-Infrared Spectroelectrochemistry of the Anion Radicals and Dianions of $C_{60}(CF_3)_{2n}$ ($2n = 2-10$) Derivatives and Density Functional Theory-Assisted Assignment

Alexey A. Popov,*[,†,‡] Ivan E. Kareev,[§] Natalia B. Shustova,[||] Steven H. Strauss,*[,||] Olga V. Boltalina,*[,||] and Lothar Dunsch*[,†]

Department of Electrochemistry and Conducting Polymers, Leibniz Institute for Solid State and Materials Research Dresden, Helmholtzstraβe 20, Dresden D01069, Germany, Chemistry Department, Moscow State University, Moscow 119992, Russia, Institute of Problems of Chemical Physics, Russian Academy of Sciences, Chernogolovka 142432, Russia, and Department of Chemistry, Colorado State University, Fort Collins, Colorado 80523

Received May 20, 2010; E-mail: a.popov@ifw-dresden.de; steven.strauss@colostate.edu; ovbolt@lamar.colostate.edu; l.dunsch@ifw-dresden.de

Abstract: The charged states of $C_{60}(CF_3)_{2n}$ ($2n = 2-10$) derivatives have been studied by electron spin resonance (ESR) and vis−near-infrared (NIR) spectroelectrochemistry. The anion radicals and diamagnetic dianions were furthermore described by theoretical calculations. The ESR spectra of anion radicals exhibit complex patterns due to multiple CF_3 groups. Their interpretation is accomplished by DFT calculations with B3LYP functional. It is shown that calculations provide reliable results when the extended aug-cc-pCVTZ basis set is used for fluorine atoms; however, specially tailored basis sets such as EPR-III also give very similar results with only a fraction of the computational cost. Absorption spectra of the anions exhibit NIR absorption bands, whose assignment is provided by time-dependent DFT calculations.

Introduction

Recent developments in fullerene perfluoroalkylation methodologies have resulted in the isolation and structural characterization of more than 100 CF_3 derivatives of C_{60},[1−9] C_{70},[10−19] and higher fullerenes.[20−26] This is the largest family of any type of derivatives known for fullerenes, providing a unique situation in fullerene chemistry with respect to the broad range of available compositions and the large number of well-characterized isomers for each composition.

Recently, we have reported an extended cyclic voltammetry study of many $C_{60}(CF_3)_{2n}$ and $C_{70}(CF_3)_{2n}$ derivatives. Because of the electron-withdrawing nature of perfluoralkyl groups, most, but not all, $C_{60,70}(CF_3)_{2n}$ compounds are stronger electron acceptors than are their parent fullerenes.[6,19,27,28] Moreover, unlike fluorofullerenes, which are also good electron acceptors but rapidly lose F atoms or F ions upon electrochemical reduction,[27,29] many $C_{60}(CF_3)_n$ compounds form stable anion radicals. Many $C_{60,70}(CF_3)_n$ compounds exhibit three reversible electrochemical reductions at modest scan rates in dichloromethane at 25 °C.[6,19] We have also found that the reduction

† Leibniz Institute for Solid State and Materials Research Dresden.
‡ Moscow State University.
§ Russian Academy of Sciences.
|| Colorado State University.

(1) Goryunkov, A. A.; Kuvychko, I. V.; Ioffe, I. N.; Dick, D. L.; Sidorov, L. N.; Strauss, S. H.; Boltalina, O. V. *J. Fluorine Chem.* **2003**, *124*, 61–64.
(2) Kareev, I. E.; Kuvychko, I. V.; Lebedkin, S. F.; Miller, S. M.; Anderson, O. P.; Seppelt, K.; Strauss, S. H.; Boltalina, O. V. *J. Am. Chem. Soc.* **2005**, *127*, 8362–8375.
(3) Kareev, I. E.; Shustova, N. B.; Kuvychko, I. V.; Lebedkin, S. F.; Miller, S. M.; Anderson, O. P.; Popov, A. A.; Strauss, S. H.; Boltalina, O. V. *J. Am. Chem. Soc.* **2006**, *128*, 12268–12280.
(4) Troyanov, S. I.; Dimitrov, A.; Kemnitz, E. *Angew. Chem., Int. Ed.* **2006**, *45*, 1971–1974.
(5) Kareev, I. E.; Shustova, N. B.; Peryshkov, D. V.; Lebedkin, S. F.; Miller, S. M.; Anderson, O. P.; Popov, A. A.; Boltalina, O. V.; Strauss, S. H. *Chem. Commun.* **2007**, 1650–1652.
(6) Popov, A. A.; Kareev, I. E.; Shustova, N. B.; Stukalin, E. B.; Lebedkin, S. F.; Seppelt, K.; Strauss, S. H.; Boltalina, O. V.; Dunsch, L. *J. Am. Chem. Soc.* **2007**, *129*, 11551–11568.
(7) Troyanov, S. I.; Goryunkov, A. A.; Dorozhkin, E. I.; Ignat'eva, D. V.; Tamm, N. B.; Avdoshenko, S. M.; Ioffe, I. N.; Markov, V. Y.; Sidorov, L. N.; Scheurel, K.; Kemnitz, E. *J. Fluorine Chem.* **2007**, *128*, 545–551.
(8) Dorozhkin, E. I.; Goryunkov, A. A.; Ioffe, I. N.; Avdoshenko, S. M.; Markov, V. Y.; Tamm, N. B.; Ignat'eva, D. V.; Sidorov, L. N.; Troyanov, S. I. *Eur. J. Org. Chem.* **2007**, *2007*, 5082–5094.
(9) Kareev, I. E.; Kuvychko, I. V.; Lebedkin, S. F.; Miller, S. M.; Anderson, O. P.; Strauss, S. H.; Boltalina, O. V. *Chem. Commun.* **2006**, 308–310.
(10) Kareev, I. E.; Kuvychko, I. V.; Popov, A. A.; Lebedkin, S. F.; Miller, S. M.; Anderson, O. P.; Strauss, S. H.; Boltalina, O. V. *Angew. Chem., Int. Ed.* **2005**, *44*, 7984–7987.
(11) Dorozhkin, E. I.; Ignat'eva, D. V.; Tamm, N. B.; Goryunkov, A. A.; Khavrel, P. A.; Ioffe, I. N.; Popov, A. A.; Kuvychko, I. V.; Streletskiy, A. V.; Markov, V. Y.; Spandl, J.; Strauss, S. H.; Boltalina, O. V. *Chem.-Eur. J.* **2006**, *12*, 3876–3889.
(12) Avdoshenko, S. M.; Goryunkov, A. A.; Ioffe, I. N.; Ignat'eva, D. V.; Sidorov, L. N.; Pattison, P.; Kemnitz, E.; Troyanov, S. I. *Chem. Commun.* **2006**, 2463–2465.

potentials of $C_{60,70}(CF_3)_{2n}$ derivatives strongly depend on their addition pattern (the difference in the reduction potentials up to 0.5 V was found for some of the isomers) and have shown that this pattern is more important than the number of the added groups.[6,19] This phenomenon has been explained by a DFT study, demonstrating that the lowest unoccupied molecular orbital (LUMO) of these derivatives has a distinct localization pattern: LUMO is always anchored to the double bonds in pentagons (DBIPs), which have two sp^2 neighbors (referred to as "non-terminal DBIPs" or just "*nt*-DBIPs"). The number of *nt*-DBIPs and their relative location was found to be the most important factor determining the shape and the energy of LUMOs and, correspondingly, of the reduction potentials of $C_{60,70}(CF_3)_{2n}$ derivatives.

The information on the LUMO localization, however, remains purely theoretical unless some experimental access to the LUMO-derived properties is provided. We have shown that the SOMO of anion radicals has essentially the same shape as the LUMO in the neutral species.[6] Because the spin density distribution in fullerene$(CF_3)_{2n}$ anion radicals is mostly determined by their SOMO, ESR spectroscopy provides a direct access to the SOMO (LUMO), and the assessment of the previously proposed conclusions on the spatial localization of LUMO is possible with this technique. However, the large number of CF_3 groups inevitably results in serious complication of the ESR spectra. In the 1990s, Morton, Preston, and co-workers reported a series of ESR studies of fullerene-based radicals, including a family of $C_{60}R_f$ radicals ($R_f = CF_3$, C_2F_5, $CF(CF_3)_2$, $C(CF_3)_3$).[30,31] Fagan et al. have also reported ESR spectra of $C_{60}C_2F_5$ and $C_{60}(CF_2)_2CF_3$ radicals.[32] With the increase of the size of the perfluoroalkyl group, the authors have observed serious complication of the ESR spectra and dynamical behavior of the radicals. In particular, hindered rotation around the bond connecting the alkyl group to the fullerene was found. Interpretation of the spectra could be fulfilled only with the use of variable-temperature ESR in the broad temperature range. In their review, Morton, Negri, and Preston have concluded that interpretation of the spectra of monoalkyl radicals of C_{60} was possible only because of the high symmetry of the adducts, which caused simplification of the spectra.[31] They have also proposed that "Detection of isomers with lower symmetry will be more difficult because of the inequivalence of the substituents and the consequent complexity of the hyperfine manifold. The inevitable result will be broad, poorly resolved spectra not readily detectable by CW-EPR. If advances are to be made in these areas, it seems likely that they will only come with the application of high-resolution EPR techniques such as ENDOR. It will not be easy, however, to make these advances, since there is the penalty of lower sensitivity to be paid for higher resolution." We have recently reported that CW-ESR spectra still could be measured for $C_{60}(CF_3)_4^-$, $C_{60}(CF_3)_{10}^-$, $C_{70}(CF_3)_2^-$, and $C_{70}(C_2F_5)_2^-$ anion radicals, which exhibited relatively narrow spectral lines. However, interpretation of the spectra was possible so far only for the anion radicals of $C_{70}(R_f)_2$. In $C_{60}(CF_3)_{2n}$ anion radicals, the more complex situation is found because their SOMO is delocalized over several carbon atoms; besides, there is no direct correlation between the spin density on the carbon atoms and hyperfine splitting values of CF_3 groups attached to the cage. Hence, the sole possibility to make an assignment of the ESR spectra of $C_{60}(CF_3)_{2n}$ anion radicals is an open question.

Anions of fullerenes and their derivatives have characteristic absorptions in the near-infrared (NIR) range,[33] and transitions assigned to these bands are often used to explain the mechanism(s) of photoinduced electron-transfer observed in transient absorption studies of fullerene-based donor−acceptor ensembles.[34] Tunable electron-accepting properties of fullerene$(R_f)_{2n}$ compounds make them attractive for use in electron-acceptor components of photovoltaic assemblies, and detailed studies of the frontier orbitals and vis−NIR transitions of their anions are essential for such applications.

In this work, we report on an extended ESR and vis−NIR spectroelectrochemical study of the $C_{60}(CF_3)_{2n}$ ($2n = 2-10$) derivatives and provide interpretations of the spectra based on the DFT calculations. We show that even very complex ESR spectra of the anion radicals of unsymmetrical fullerene derivatives can be interpreted with the help of extended DFT calculations.

Experimental Details

Synthesis and isolation of $C_{60}(CF_3)_{2n}$ derivatives were reported elsewhere (see ref 6 and references therein). A new isomer of $C_{60}(CF_3)_{10}$ was isolated in this work in the course of purification of $C_{60}(CF_3)_{10}$-1 reported by us earlier.[6] Using the HPLC method

(13) Ignat'eva, D. V.; Goryunkov, A. A.; Tamm, N. B.; Ioffe, I. N.; Avdoshenko, S. M.; Sidorov, L. N.; Dimitrov, A.; Kemnitz, E.; Troyanov, S. I. *Chem. Commun.* **2006**, 1778–1780.
(14) Dorozhkin, E. I.; Ignat'eva, D. V.; Tamm, N. B.; Vasilyuk, N. V.; Goryunkov, A. A.; Avdoshenko, S. M.; Ioffe, I. N.; Sidorov, L. N.; Pattison, P.; Kemnitz, E.; Troyanov, S. I. *J. Fluorine Chem.* **2006**, *127*, 1344–1348.
(15) Goryunkov, A. A.; Ignat'eva, D. V.; Tamm, N. B.; Moiseeva, N. N.; Loffe, I. N.; Avdoshenko, S. M.; Markov, V. Y.; Sidorov, L. N.; Kemnitz, E.; Troyanov, S. I. *Eur. J. Org. Chem.* **2006**, 2508–2512.
(16) Kareev, I. E.; Lebedkin, S. F.; Miller, S. M.; Anderson, O. P.; Strauss, S. H.; Boltalina, O. V. *Acta Crystallogr., Sect. E.* **2006**, *62*, O617–O619.
(17) Kareev, I. E.; Lebedkin, S. F.; Miller, S. M.; Anderson, O. P.; Strauss, S. H.; Boltalina, O. V. *Acta Crystallogr., Sect. E.* **2006**, *62*, O620–O622.
(18) Tamm, N. B.; Troyanov, S. I. *Mendeleev Commun.* **2007**, *17*, 172–174.
(19) Popov, A. A.; Kareev, I. E.; Shustova, N. B.; Lebedkin, S. F.; Strauss, S. H.; Boltalina, O. V.; Dunsch, L. *Chem.-Eur. J.* **2007**, *14*, 107–121.
(20) Shustova, N. B.; Kuvychko, I. V.; Bolskar, R. D.; Seppelt, K.; Strauss, S. H.; Popov, A. A.; Boltalina, O. V. *J. Am. Chem. Soc.* **2006**, *128*, 15793–15798.
(21) Shustova, N. B.; Newell, B. S.; Miller, S. M.; Anderson, O. P.; Bolskar, R. D.; Seppelt, K.; Popov, A. A.; Boltalina, O. V.; Strauss, S. H. *Angew. Chem., Int. Ed.* **2007**, *46*, 4111–4114.
(22) Kareev, I. E.; Kuvychko, I. V.; Shustova, N. B.; Lebedkin, S. F.; Bubnov, V. P.; Anderson, O. P.; Popov, A. A.; Boltalina, O. V.; Strauss, S. H. *Angew. Chem., Int. Ed.* **2008**, *47*, 6204–6207.
(23) Kareev, I. E.; Popov, A. A.; Kuvychko, I. V.; Shustova, N. B.; Lebedkin, S. F.; Bubnov, V. P.; Anderson, O. P.; Seppelt, K.; Strauss, S. H.; Boltalina, O. V. *J. Am. Chem. Soc.* **2008**, *130*, 13471–13489.
(24) Tamm, N. B.; Sidorov, L. N.; Kemnitz, E.; Troyanov, S. I. *Chem.-Eur. J.* **2009**, *15*, 10486–10492.
(25) Troyanov, S. I.; Tamm, N. B. *Crystallogr. Rep.* **2009**, *54*, 598–602.
(26) Troyanov, S. I.; Tamm, N. B. *Chem. Commun.* **2009**, 6035–6037.
(27) Popov, A. A.; Tarabek, J.; Kareev, I. E.; Lebedkin, S. F.; Strauss, S. H.; Boltalina, O. V.; Dunsch, L. *J. Phys. Chem. A* **2005**, *109*, 9709–9711.
(28) Popov, A. A.; Shustova, N. B.; Boltalina, O. V.; Strauss, S. H.; Dunsch, L. *ChemPhysChem* **2008**, *9*, 431–438.
(29) Zhou, F. M.; Vanberkel, G. J.; Donovan, B. T. *J. Am. Chem. Soc.* **1994**, *116*, 5485–5486.
(30) Morton, J. R.; Preston, K. F. *J. Phys. Chem.* **1994**, *98*, 4993–4997.
(31) Morton, J. R.; Negri, F.; Preston, K. F. *Acc. Chem. Res.* **1998**, *31*, 63–69.
(32) Fagan, P. J.; Krusic, P. J.; McEwen, C. N.; Lazar, J.; Parker, D. H.; Herron, N.; Wasserman, E. *Science* **1993**, *262*, 404–407.
(33) Reed, C. A.; Bolskar, R. D. *Chem. Rev.* **2000**, *100*, 1075–1119.
(34) Segura, J. L.; Martin, N.; Guldi, D. *Chem. Soc. Rev.* **2005**, *34*, 31–47.

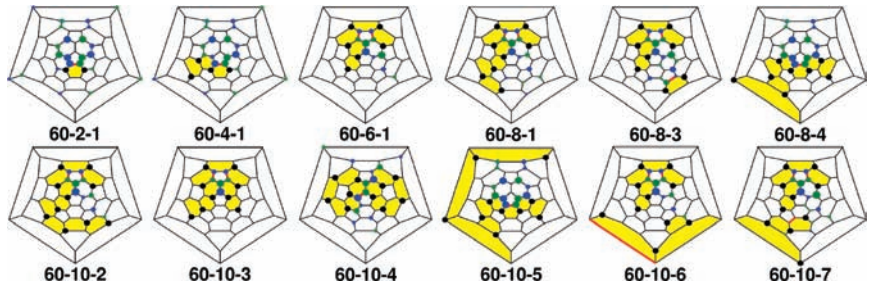

Figure 1. Schlegel diagrams of the $C_{60}(CF_3)_{2n}$ derivatives studied in this work. Black circles denote positions of CF_3 groups, blue and green circles show localization of LUMO, nt-DBIPs are highlighted in red, and ribbons of the edge-sharing *meta*- or *para*-$C_6(CF_3)_2$ hexagons are highlighted in yellow.

(10 mm i.d. × 250 mm Buckyprep Cosmosil column (Nacalai Tesque Co.)), the fraction containing mostly $C_{60}(CF_3)_{10}$-1 was processed using 100% heptanes as eluent at a 5 mL/min flow rate; the main component was eluted at 7.7 min and was confirmed by NMR as $C_{60}(CF_3)_{10}$-1, and a smaller peak eluting at 9.6 min was collected. The negative-ion APCI-mass spectrum indicated molecular composition $C_{60}(CF_3)_{10}$ with *m*/*z* 1410. The ^{19}F NMR spectrum (see the Supporting Information, Figure S-1) in $CDCl_3$ (C_6F_6 internal standard, $-\delta$ 164.9) showed 10 resonances of equal intensities: $-\delta$ (J_{FF}): 74.8 (q, 9.8), 72.9 (q, 11.3), 70.8 (q, 14.7), 69.9 (q, 13.9), 68.9 (m), 68.6 (m), 67.9 (m), 67.3 (m), and 66.7 (m). The fluorine-19 NMR spectrum was recorded at 25 °C using a Varian INOVA-unity 400 spectrometer operating at 376.5 MHz. A small amount of hexafluorobenzene was added as an internal standard (δ −164.9). APCI mass spectra were recorded using a ThermQuest Finnagan LCQ-DUO spectrometer.

Cyclic voltammetry was carried out in a glovebox (water and oxygen content bellow 1 ppm) in a one-compartment electrochemical cell. The electrolyte solution was 0.1 M N(*n*-Bu)$_4$BF$_4$ (TBABF$_4$) in dichloromethane or in *o*-dichlorobenzene (*o*-DCB). Platinum wire (or plate), platinum wire loop, and a silver wire served as working, counter, and pseudoreference electrodes, respectively. The potentials were measured as referred to the $Fe(Cp)_2^{+/0}$ or $Fe(Cp^*)_2^{+/0}$ couple; that is, $Fe(Cp)_2$ was added as the internal standard at the end of the voltammetric measurements, which were controlled by a PAR 273 potentiostat/galvanostat.

The spectroelectrochemical cell with a laminated Pt-mesh working electrode, a Pt-wire counter electrode, and a silver wire quasi-reference electrode was described in detail earlier.[35,36] The cell was filled with a solution of the fullerene compound under study in the glovebox, then tightly closed and transferred into the optical cavity (ER4104OR, Bruker, Germany) of the X-band ESR spectrometer (EMX Bruker, Germany) for spectroelectrochemical measurements. The optical cavity has two openings for the optical cables connecting the sources and detectors of the UV−vis−NIR spectrometer (TIDAS, J&M, Germany) with the cavity. Cyclic voltammetry in spectroelectrochemical measurements was controlled by the HEKA potentiostat/galvanostat system (HEKA Elektronik, Germany).

When the amount of the radicals generated in situ was not sufficient for the highly resolved ESR spectra, chemical reduction of the studied compounds by 1 equiv of cobaltocene in *o*-DCB was used (we did not find any noticeable differences of the ESR spectra measured in CH_2Cl_2 and *o*-DCB solution). With chemically reduced species, long integration time for the registration of the ESR spectra was possible. Absorption spectra of the chemically generated monoanions were measured using a Shimadzu 3100 spectrophotometer. The ESR and vis−NIR spectra of the chemically reduced $C_{60}(CF_3)_{2n}$ derivatives did not change for at least one day, pointing to a high stability of these species in the absence of air. However, the spectra changed immediately when air was bubbled through the solution.

Computational Details

The structures of $C_{60}(CF_3)_{2n}$ compounds in all charged states are optimized at the PBE[37]/TZ2P level using the PRIRODA[38] package; the code employed expansion of the electron density in an auxiliary basis set to accelerate evaluation of the Coulomb and exchange-correlation terms.[39] Point-energy calculations at the B3LYP level with the 6-311G* basis set for carbon atoms and various basis sets for fluorine atoms are performed using the Firefly package.[40] For radicals, spin unrestricted calculations were performed in most cases, and this option is taken as default hereafter. When restricted-orbital (RO) calculations are also performed in special cases, it is denoted explicitly.

Time-dependent DFT calculations were performed at the PBE/Λ01 level using the PRIRODA package and PBE/TZ2P-optimized structures (Λ01 is a DZVP-quality basis set developed by Laikov;[41] testing calculations have shown that the use of more extended basis sets resulted in a slight shift of excitation energies; however, the whole spectral pattern remained the same).

Simulation of the ESR spectra and fitting procedures were performed using Winsim v.1.0.[42] Visualization of spin density distribution was done with ChemCraft.[43]

Results and Discussion

Studied Compounds. The Schlegel diagrams with schematic LUMO (SOMO) distribution of the $C_{60}(CF_3)_{2n}$ ($2n = 2-10$) compounds studied in this work are shown in Figure 1. To denote the compounds, we will use the following abbreviation adopted from refs 6, 19: each $C_{60}(CF_3)_{2n}$ compound is denoted as **60-2*n*-*N***, where **2*n*** is the number of CF_3 groups, while ***N*** is the number of the isomer (from ref 6). For instance, the third isomer of $C_{60}(CF_3)_{10}$ is **60-10-3** in this notation.

(35) Petr, A.; Dunsch, L.; Neudeck, A. *J. Electroanal. Chem.* **1996**, *412*, 153–158.
(36) Rapta, P.; Bartl, A.; Gromov, A.; Stasko, A.; Dunsch, L. *ChemPhysChem* **2002**, *3*, 351–356.
(37) Perdew, J. P.; Burke, K.; Ernzerhof, M. *Phys. Rev. Lett.* **1996**, *77*, 3865–3868.
(38) Laikov, D. N.; Ustynuk, Y. A. *Russ. Chem. Bull.* **2005**, *54*, 820–826.
(39) Laikov, D. N. *Chem. Phys. Lett.* **1997**, *281*, 151–156.
(40) Granovsky, A. A. PC GAMESS/Firefly, version 7.1.C, http://classic.chem.msu.su/gran/gamess/index.html. PC GAMESS/Firefly, version 7.1.C, *http://classic.chem.msu.su/gran/gamess/index.html*, 2008.
(41) Laikov, D. N. *Chem. Phys. Lett.* **2005**, *416*, 116–120.
(42) O'Brien, D. A.; Duling, D. R.; Fann, Y. C. EPR Spectral Simulation for MS-Windows, Public EPR Software Tools, National Institute of Environment Health Sciences, National Institutes of Health, U.S., http://epr.niehs.nih.gov, 2002.
(43) Zhurko, G. A. ChemCraft, version 1.6, http://www.chemcraftprog.com, 2009.

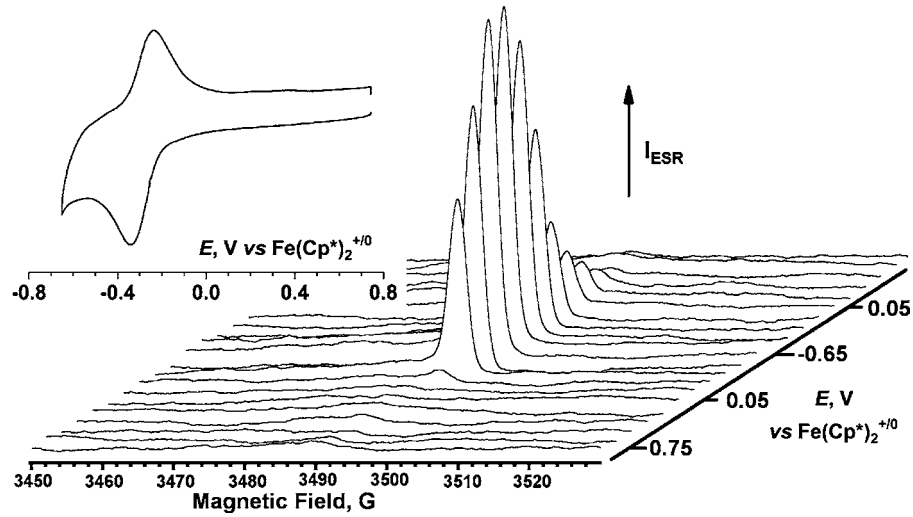

Figure 2. Typical result of the in situ ESR spectrolectrochemical measurement. The figure shows changes of the integrated ESR signal with the potential during cyclic voltammetry of **60-4-1** at the first reduction (cyclic voltammogram is shown in the inset).

Trifluoromethyl groups are sterically bulky (they are significantly larger than iodine atoms, for example[44,45]), and of the $C_{60}(CF_3)_{2n}$ compounds with $2n \leq 10$, only one structure, **60-6-2**, is known to have two CF_3 groups on adjacent cage carbon atoms.[3] 1,4-Addition appears to be the rule for CF_3 groups, and most of the fullerene$(CF_3)_n$ compounds have a common addition pattern, which includes a ribbon of edge-sharing *meta*- and/or *para*-$C_6(CF_3)_2$ hexagons (**60-4-1** has a *para*−*meta*−*para* or *pmp* ribbon, **60-6-1** has a *para*−*para*−*para*−*meta*−*para* or p^3mp ribbon, **60-8-1** has a p^3mpmp ribbon, **60-8-4** has a *pmpmpmp* ribbon, **60-10-2** has a $p^3mpmpmp$ ribbon, and **60-10-5** has a *pmpmpmpmp* ribbon; such patterns can be envisaged as a result of subsequent 1,4-additions). In some cases, a ribbon plus an isolated *p*-$C_6(CF_3)_2$ hexagon (**60-8-3** has p^3mp,*p* addition pattern) or two ribbons with even number of CF_3 groups (**60-10-6** has a p^3mp,*pmp*) are formed.

The compounds studied in this work can be divided into two groups on the basis of the number of *nt*-DBIPs. One group (**60-2-1**, **60-4-1**, **60-8-4**, and **60-10-5**) includes the compounds with one *nt*-DBIP. These compounds have acenaphthalene-like LUMO, and the first reduction potential shifted cathodically by ca. 0.1 V with respect to the $C_{60}^{0/-}$ pair. Another group includes the compounds with two *nt*-DBIPs in one pentagon (**60-6-1**, **60-8-1**, **60-8-3**, **60-10-2**, **60-10-3**, and **60-10-6**; all of these compounds have p^3 fragment in the ribbon). These compounds have fulvene-like LUMO and the first reduction potential of ca. 0.3 V versus $C_{60}^{0/-}$. Note that while **60-8-3** and **60-10-5** have also the third *nt*-DBIP formed either by the isolated *p*-$C_6(CF_3)_2$ hexagon (**60-8-3**) or by the *pmp* ribbon (**60-10-5**), their LUMO is still determined by the p^3 fragment with two *nt*-DBIPs. **60-10-4** is a special case in that it has two *nt*-DBIPs in different pentagons.

Molecular Structure of 60-10-7. In addition to the derivatives with well-known structures, we have also studied one new isomer of $C_{60}(CF_3)_{10}$ (**60-10-7** hereafter). The ^{19}F NMR spectrum showed 10 resonances with equal intensities in the $-\delta$ range of 66−75 ppm. Four of the resonances are quartets with J_{FF} values between 9.8 and 14.7 Hz, indicating that two different ribbons should be present in the structure. We rule out the possibility of the presence of an isolated pair of CF_3 groups sharing the same hexagon, because there is no pair of the quartets that have the same coupling constants. Formation of two ribbons with odd numbers of CF_3 groups (e.g., 5 + 5 or 3 + 7) is not typical for $C_{60}(CF_3)_{2n}$ compounds. Therefore, an addition pattern with two ribbons consisting of four and six CF_3 groups can be regarded as most probable. We previously structurally characterized an isomer with such an addition pattern, $C_{60}(CF_3)_{10}$ (**60-10-6**).[6,46] DFT calculations revealed several stable isomers with (4 + 6) addition patterns. Cyclic voltammetry of **60-10-7** has shown that this compound exhibits two reversible reductions at 0.28 and −0.36 V versus $C_{60}^{0/-}$ couple in *o*-DCB solution at room temperature. At higher scan rates (5−10 V s^{-1}), the third reduction step at −0.98 V can be observed as well. In ref 6, we have found an excellent correlation between the LUMO energies and reduction potentials of $C_{60}(CF_3)_{2n}$ derivatives, which can be used to verify their isomeric structure. We have found that among the low-energy isomers of $C_{60}(CF_3)_{10}$ with 6 + 4 addition patterns, only the isomer, the Schlegel diagram of which is shown in Figure 1, has a suitable LUMO energy to match the measured reduction potential (see the Supporting Information for more details).

ESR Measurements. Typical results of the in situ ESR spectroelectrochemical measurements are shown in Figure 2 for **60-4-1**. There is a strong increase of the ESR intensity at the potential of the first reduction of the studied compound (see inset in Figure 2 for the cyclic voltammetry at the first reduction step); the signal continues to grow in the potential range beyond the reoxidation potential of the anion radical, and when this potential is reached at the back scan, the ESR intensity starts to decrease, reaching almost zero at the end of the measurement. This method establishes the direct link between the redox state of the studied compound and spectroscopic response and hence enables an unambiguous attribution of the ESR spectra to the radical species generated at certain reduction or oxidation steps.[28,36] However, in some cases, the concentration of the radical species formed was not sufficiently high for a detailed

(44) Charton, M. *J. Am. Chem. Soc.* **1969**, *91*, 615–618.
(45) Bott, G.; Field, L. D.; Sternhell, S. *J. Am. Chem. Soc.* **1980**, *102*, 5618–5626.
(46) Shustova, N. B.; Peryshkov, D. V.; Popov, A. A.; Boltalina, O. V.; Strauss, S. H. *Acta Crystallogr., Sect. E* **2007**, *63*, O3129–U2823.

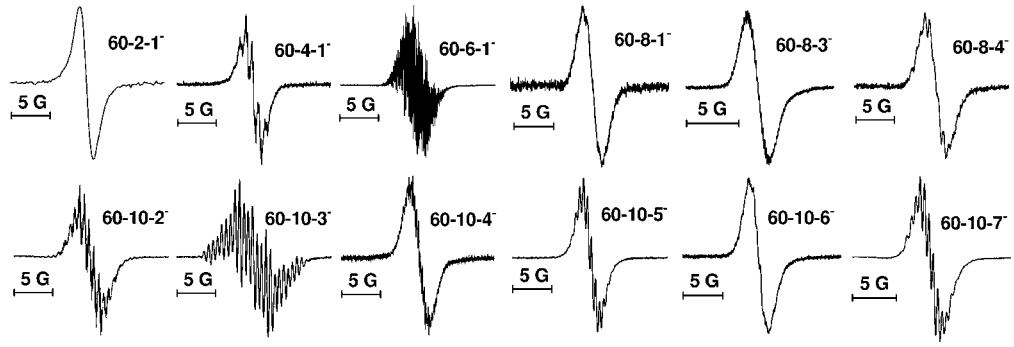

Figure 3. Overview of the ESR spectra of the $C_{60}(CF_3)_{2n}^-$ anion radicals.

study of the spectra with low modulation amplitude (which is necessary to obtain the well-resolved spectra but results in the decrease of the signal-to-noise ratio). In such cases, radicals were generated in parallel by the chemical reaction with ca. 1 equiv of cobaltocene and then studied by ESR ex situ. Comparison of the results of the two techniques ensures that the species observed ex situ are the same species that are formed at the first reduction step, that is, are the genuine anion radicals of the studied compounds.

Figure 3 shows the survey of the ESR spectra of the anion radicals of selected $C_{60}(CF_3)_{2n}$ derivatives. $C_{60}(CF_3)_{2n}^-$ radicals exhibit the ESR spectra with the halfwidth of ca. 3−5 G. Hyperfine coupling constants of the $C_{60}(CF_3)_{2n}^-$ radicals are less than 2 G, which is comparable to the values normally observed for the $C_{60}R_f$ radicals.[30−32,47] In many cases, the hyperfine structure is superimposed by the broad line, but in several cases (**60-4-1**, **60-6-1**, **60-10-2**, **60-10-3**, **60-10-5**, **60-10-7**), well-resolved spectra with narrow lines can be observed, and these spectra and their interpretation will be the main focus of this work. The fact that relatively narrow ESR lines (halfwidth of ca. 0.1 G) can be also observed in the spectra of **60-10-4** and **60-8-3** shows that experimental resolution and concentration were sufficient for the spectra to be measured, and the fact that the ESR lines are still rather broad is due to the intrinsic property of these radicals at room temperature rather than to inappropriate conditions for spectra acquisition. An unambiguous interpretation of the hfc pattern of such spectra is hardly possible because of numerous sets of hfc constants, which would result in the broad line without any hint of hyperfine structure, and hence they will not be discussed in detail hereafter.

Interpretation of the ESR spectra of the anion radicals of trifluoromethylated fullerenes meets intrinsic difficulties because of the complexity of the studied molecules. Most of these compounds are nonsymmetric, resulting in a specific hyperfine splitting pattern of each CF_3 group. Because the studied derivatives have up to 10 CF_3 groups, very complex spectra can be expected (and are indeed observed). However, the interpretation is somewhat simplified by the fact that CF_3 groups rotate rapidly at room temperature at the ESR time-scale,[28,30] and hence only one hfc constant is necessary to describe one CF_3 group.

Assessment of DFT Calculations. The hyperfine coupling constants of the complex systems are not available straightforward from the ESR spectra, and only simulation of the spectra can be used to judge if the set of the proposed hfc constants provides a good match to the experimental spectrum. Moreover, for the radicals like those studied in this work, in which several hfc constants can be very similar, fitting is necessary to obtain individual hfc constants for all CF_3 groups. However, the fitting is an inverse problem solution, which is known to be ill-defined in most cases (that is, different solutions are possible, and the use of different initial parameters for the simulation can result in different resulting hfc constants obtained in the fitting procedure; in addition, we have observed that even a small variation of hfc values can drastically affect simulated spectra). Hence, a reliable theoretical approach is needed, which can provide reasonable hfc constants of CF_3 groups for the initial set in the fitting procedure so that these constants are close to the final solution and should not be significantly varied in the fitting procedure. Once this condition is fulfilled, one can ensure that the values obtained in the fitting procedure have a solid physical background. While modern ab initio approaches such as CCSD can provide hyperfine coupling constants with very high accuracy,[48] the use of such methods for the fullerene derivatives is still impossible because of the large size and low symmetry of the $C_{60}(CF_3)_{2n}$ anion radicals. Hence, we are limited to the use of DFT approaches. For the computations of hfc constants in this work, we use PBE/TZ2P-optimized coordinates, because this method, on the one hand, is computationally feasible within the use of density fitting technique[39] and, on the other hand, provides a good description of the experimental structural parameters of CF_3 derivatives of fullerenes.[5,6,21] Hyperfine coupling constants are then computed using the B3LYP functional. A series of test calculations were performed using different basis sets for the fluorine atoms, including 6-311G*, cc-pVTZ, cc-pCVTZ, aug-cc-pCVTZ, as well as the basis sets specially tailored for the prediction of the core properties such as IGLO-II, IGLO-III,[49] EPR-II, and EPR-III[50] (here II and III stand for the double-ζ and triple-ζ basis sets). Table 1 lists averaged hfc constants for CF_3 groups in **60-4-1**$^-$ and **60-6-1**$^-$ as compared to the "experimental" constants. By experimental values here, we understand the constants obtained in the fitting procedure with aug-cc-pCVTZ predicted hfc constants as starting parameters (a more detailed description of the hfc constants of **60-4-1**$^-$ and **60-6-1**$^-$ is given below).

(47) Goryunkov, A. A.; Kornienko, E. S.; Magdesieva, T. V.; A., K. A.; Vorobiev, V. A.; Avdoshenko, S. M.; Ioffe, I. N.; Nikitin, O. M.; Markov, V. Y.; Khavrel, P. A.; Vorobiev, A. K.; Sidorov, L. N. *Dalton Trans.* **2008**, 6886–6893.

(48) Improta, R.; Barone, V. *Chem. Rev.* **2004**, *104*, 1231–1253.

(49) Kutzelnigg, W.; Fleischer, U.; Schnidler, S. The IGLO-Method: Ab Initio Calculation and Interpretation of NMR Chemical Shifts and Magnetic Susceptibilities. *NMR Basic Principles and Progress*; Springer Verlag: Berlin/Heidelberg, 1991; pp 165−262.

(50) Barone, V. Structure, Magnetic Properties and Reactivities of Open-Shell Species from Density Functional and Self-Consistent Hybrid Methods. In *Recent Advances in Density Functional Methods*; Chong, D. P., Ed.; World Scientific: Singapore, 1995; p 287.

Table 1. Hyperfine Coupling Constants of CF_3 Groups in **60-4-1**$^-$ and **60-6-1**$^-$ Computed at the U-B3LYP Level with Different Basis Sets for Fluorine Atoms and Measured Experimentally and Correlations between the Values[a]

		calc. (basis set)									
	group	6-311G*	IGLO-II	IGLO-III	EPR-II	EPR-III	cc-pVTZ	cc-pCVTZ	RO/aug-cc-pCVTZ[b]	aug-cc-pCVTZ	exp.
60-4-1	CF_3-3	0.691	0.750	0.823	0.869	0.860	0.702	0.752	0.648	0.846	0.760
	CF_3-2	0.616	0.698	0.765	0.793	0.790	0.684	0.709	0.643	0.792	0.760
	CF_3-1	0.215	0.252	0.292	0.308	0.311	0.249	0.252	0.281	0.314	0.210
	CF_3-4	0.145	0.161	0.171	0.171	0.170	0.150	0.171	0.175	0.166	0.210
60-6-1	CF_3-2	0.866	1.001	1.073	1.116	1.110	0.958	1.000	0.863	1.101	1.094
	CF_3-5	0.766	0.849	0.894	0.914	0.904	0.794	0.872	0.747	0.903	0.919
	CF_3-3	0.461	0.513	0.546	0.558	0.560	0.505	0.521	0.473	0.552	0.594
	CF_3-4	0.270	0.317	0.347	0.371	0.368	0.275	0.311	0.310	0.357	0.348
	CF_3-6	0.175	0.230	0.255	0.267	0.269	0.225	0.229	0.239	0.270	0.244
	CF_3-1	0.125	0.142	0.155	0.150	0.147	0.098	0.157	0.194	0.141	0.163
SF(aug-cc-pCVTZ)[c]		1.2445	1.1037	1.0242	0.9868	0.9928	1.1601	1.0919	1.2270		
R^2(aug-cc-pCVTZ)[c]		0.9905	0.9961	0.9991	0.9995	0.9997	0.9948	0.9932	0.9819		
SF(exp.)[d]		1.2157	1.0781	0.9992	0.9620	0.9678	1.1329	1.0671	1.1978	0.9747	
R^2(exp.)[d]		0.9857	0.9906	0.9846	0.9796	0.9792	0.9871	0.9916	0.9725	0.9786	

[a] All hfc values are in gauss; for each compound, the values are listed in descending order. [b] Results of the RO-B3LYP/aug-cc-pCVTZ calculation. [c] For a given basis set, SF(aug-cc-pCVTZ) is a scaling factor obtained from the least-squares fitting of the equation a(aug-cc-pCVTZ) = SF·a(basis set), while R^2(aug-cc-pCVTZ) is a square of the R-factor of the correlation. [d] The same as footnote c, but correlation is between computed and experimental values.

60-4-1$^-$ and **60-6-1**$^-$ were chosen as standards because (i) they have smaller number of CF_3 groups than $C_{60}(CF_3)_{10}$ isomers and hence interpretation can be easier, and (ii) their spectra exhibit fine resolution, which means that restriction on the inverse problem is strict enough to minimize the possibility of multiple solutions. A good agreement between experimental and simulated spectra confirms the validity of the proposed hfc constants for **60-4-1**$^-$ and **60-6-1**$^-$.

First, we compare results of DFT calculations with different basis sets, while a comparison of the calculated and experimental values is given in the next paragraph. Table 1 lists the results of statistical analysis of the linear correlation between hfc constants predicted using the aug-cc-pCVTZ basis set (chosen for a standard as the most extended basis set used in this work) and those computed using the other basis sets. There is a good linear correlation between all sets of hfc constants. However, the 6-311G* basis set exhibits the smallest R^2 coefficient, 0.9905, and requires the largest scaling factor, 1.2445, to match the aug-cc-pCVTZ values. The constants computed with the cc-pVTZ basis set are closer to the aug-cc-pCVTZ values, but the addition of the core-polarization or diffuse functions still noticeably alters the results of calculations. The use of the specially tailored basis set results in a better agreement with aug-cc-pCVTZ values. For instance, the comparably modest EPR-II basis set already reproduces aug-cc-pCVTZ values with very good correlation ($R^2 = 0.9995$, scaling factor 0.9868), while hfc constants predicted by the EPR-III basis set are almost indistinguishable from the aug-cc-pCVTZ values despite the smaller number of basis functions used. Similar results are observed for the IGLO-II and IGLO-III basis sets: good correlation ($R^2 = 0.9961$) is observed already for the IGLO-II basis set, while the further extension to IGLIO-III results in even better correlation ($R^2 = 0.9991$). At the same time, the constants computed with IGLO basis sets are systematically smaller than the aug-cc-pCVTZ counterparts and require the use of scaling factors of 1.112 and 1.027 for IGLO-II and IGLO-III, respectively. It should be noted that the constants computed with IGLO-II basis set are very close to the values obtained with the cc-pCVTZ basis set (R^2 correlation coefficient between the two sets is 0.9995, and the scaling factor is 1.006). It is quite remarkable that the specially tailored basis sets exhibit a faster convergence of the predicted hyperfine coupling constants with the basis set size as compared to the general-purpose basis sets, and that such moderate basis sets as EPR-II or IGLO-II can reproduce the values of the more extended basis sets with the only a fraction of cost, the facts not of the least importance for the prediction of hyperfine splitting constants of large radicals.

Comparison of the computed and experimental values is more controversial. The scaling factors necessary to reproduce the experimental hyperfine splitting constants and the correlation coefficients are listed in Table 1. Earlier we have already reported that the use of the simple 6-311G* basis set provides a reasonable estimation of the ^{19}F hfc constants of **60-4-1**$^-$ and **60-10-2**$^-$, resulting in good overall agreement between experimental and computed ESR spectra. However, a systematic deviation of ca. 15% was found for this basis set. In this work, we have found that for **60-4-1**$^-$ and **60-6-1**$^-$, 6-311G* values exhibit the worst correlation coefficient, 0.9857, and require the largest scaling factor, 1.216. Extension of the basis sets results in the approaching of the scaling factors to 1, especially for the EPR-III, aug-cc-pCVTZ, and IGLO-III basis sets, the latter showing the smallest systematic deviation with the scaling factor of 0.999. At the same time, correlation coefficients for EPR-III and aug-cc-pCVTZ basis sets are comparably poor, 0.9792 and 0.9786, respectively, while the best correlation is found for IGLO-II and cc-pCVTZ basis sets ($R^2 = 0.9906$ and 0.9916, respectively), which however require the use of the scaling factors of 1.078 and 1.067, respectively. Closer inspection of the experimental values shows that the main reason for the relatively poor efficiency of extended basis sets is because of the inadequate prediction of the hfc constants of **60-4-1**$^-$, while the values of **60-6-1**$^-$ are predicted with high accuracy. For the former, the best fit to the experimental spectra is obtained by two hfc constants, one for each pair of CF_3 groups, while calculations predict different values for all four groups. The methods that predict the smallest deviations within the pairs (IGLO-II and cc-pCVTZ) exhibit the smallest deviation of R^2 coefficient from unity. The fact that the best results are not obtained with the most extended basis sets indicates that other systematic errors might be important as well (e.g., the errors in prediction of optimized coordinates, or the intrinsic errors in the DFT). The good results obtained with smaller basis sets are probably due to the fortuitous cancellation of errors. In the view

Table 2. Hyperfine Coupling Constants (gauss) of CF_3 Groups in **60-6-1**$^-$ Computed at the U-DFT Level with Different Density Functionals and EPR-III Basis Sets for Fluorine Atoms

	group	B3LYP	B3PW91	X3LYP	O3LYP	PBE0	BHHLYP	BLYP	PBE	exp.
60-6-1	CF_3-2	1.110	1.002	1.122	1.072	1.016	1.051	1.129	1.028	1.094
	CF_3-5	0.904	0.779	0.915	0.834	0.786	0.980	0.884	0.740	0.919
	CF_3-3	0.560	0.523	0.559	0.578	0.518	0.428	0.626	0.590	0.594
	CF_3-4	0.368	0.309	0.375	0.326	0.315	0.419	0.345	0.281	0.348
	CF_3-6	0.269	0.235	0.265	0.310	0.221	0.167	0.386	0.347	0.244
	CF_3-1	0.147	0.107	0.132	0.143	0.061	0.035	0.244	0.157	0.163
SF(exp.)[a]		1.001	1.126	0.993	1.039	1.118	1.018	0.963	1.086	
R^2(exp.)[a]		0.996	0.993	0.994	0.987	0.982	0.917	0.963	0.950	

[a] For a given density functional, SF(exp.) is a scaling factor obtained from the least-squares fitting of the equation a(exp.) = SF·a(functional) for **60-6-1**$^-$, while R^2(exp.) is a square of the R-factor of the correlation.

of these findings, we will use the results of calculations with EPR-III basis sets in the following analysis of the EPR spectra of $C_{60}(CF_3)_{10}^-$ isomers.

Following a suggestion by an anonymous referee, in addition to the basis set dependence, we have also analyzed how the results of hfc calculations depend on the particular form of the density functional. For this, we have computed hfc values of **60-6-1**$^-$ using EPR-III basis set and various density functionals. To separately analyze the role of exchange and correlations functionals, we have used the same functional form as in B3LYP (so-called "ACM3"), but with the PW91[51] correlation functional on one side (B3PW91) and with the optimized Handy−Cohen[52] ("O") and Xu−Goddard[53] ("X") exchange functionals in combination with LYP[54] on the other side (i.e., O3LYP and X3LYP). The influence of exact exchange (EEX) term in functional was studied by employing the pure GGA functional BLYP (0% EEX) versus B3LYP (20% EEX) versus BHHLYP (50% EEX) versus Hartree−Fock (HF, 100% EEX); note also that the fractions of EEX in O3LYP and X3LYP are 12% and 22%, respectively. Finally, PBE0 and PBE functionals were also analyzed. Results of these calculations are presented in Table 2; to estimate the quality of the DFT results, we again estimated the scaling factor and R^2 coefficient of the linear correlation. Table 2 shows that for **60-6-1**$^-$, B3LYP provides the best agreement with experimental data (SF = 1.001, R^2 = 0.996). B3PW91 underestimates the value by ca. 10%, but when scaled by the uniform factor of 1.126, predicted values are in reasonable agreement with experiment (R^2 = 0.993). Results of the X3LYP calculations are close to B3LYP, but agreement is slightly worse (SF = 0.993, R^2 = 0.994), while O3LYP yields noticeably (but not dramatically) different results (SF = 1.039, R^2 = 0.987). In general, within ACM3 methods, both correlation and exchange functionals appear to be important, although results of different functionals are not drastically different. When the hybrid PBE0 functional is used, predicted hfc values are underestimated (SF = 1.118), while correlation between experimental and computed values is worse (R^2 = 0.982). Increase of the EEX fraction in the functional significantly worsens the results and leads to large spin contaminations: while standard hybrid functionals discussed above give an S^2 value of 0.76−0.77 (instead of the ideal 0.75), BHHLYP give an S^2 = 0.84, and correlation between experimental and computed hfc values is rather poor (R^2 = 0.917). Furthermore, unrestricted HF calculations yielded giant spin contamination (S^2 = 7.44), and hence results of hfc calculations

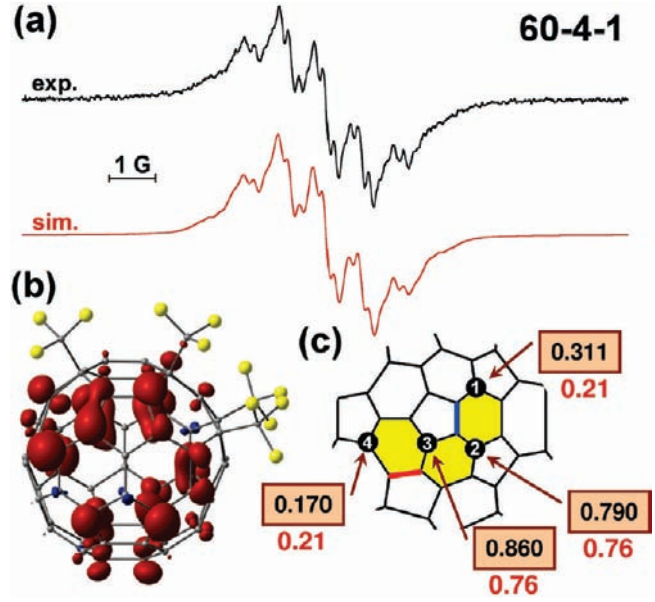

Figure 4. (a) Experimental and simulated ESR spectra of **60-4-1**$^-$; (b) spin density distribution in **60-4-1**$^-$; and (c) fragment of the Schlegel diagram of **60-4-1**$^-$ with DFT-calculated (black numbers in light-brown boxes) and experimental (red numbers) hfc constants (in gauss). The numbers of CF_3 groups used in the discussion are given in white inside black circles (note that these are not IUPAC numbers; see ref 6 for the IUPAC numbering in these derivatives).

are absolutely unreliable and are not discussed further. On the other hand, BLYP (with 0% EEX) has an S^2 of 0.75, but predicted hfc values are somewhat overestimated (SF = 0.963), and agreement with experiment (R^2 = 0.963) is not as good as for B3LYP. PBE also gives poor correlation (R^2 = 0.950) with underestimated hfc values (SF = 1.086). Thus, results of these calculations show that the hybrid functional with moderate fraction of exact exchange term (20−25%) provides the best agreement with experimental values and that B3LYP appears to be the best functional for prediction of hfc values in $C_{60}(CF_3)_{2n}^-$ anion radicals, at least with the EPR-III basis set.

Nature of the Hyperfine Splitting in $C_{60}(CF_3)_{2n}^-$ Anion Radicals. Our earlier work on the electrochemical properties of the trifluoromethylated fullerenes has shown that the LUMO (SOMO in anion radicals) of these compounds is localized on the π-system of the carbon cage with small contributions from the C-sp^3 atoms of the CF_3 groups. It is not surprising that the same spatial distribution is found for the spin density in the anion radicals as can be seen in Figure 4 for **60-4-1**$^-$. There is no apparent contribution of fluorine atoms to the spin density, and this fact raises the question of the nature of the fluorine-based hyperfine splitting observed in the $C_{60}(CF_3)_{2n}^-$ anion

(51) Perdew, J. P. PW91. In *Electronic Structure of Solids 91*; Ziesche, P., Eschrig, H., Eds.; Akademie Verlag: Berlin, 1991; p 11.
(52) Handy, N. C.; Cohen, A. J. *Mol. Phys.* **2001**, *99*, 403–412.
(53) Xu, X.; Goddard, W. A., III. *Proc. Natl. Acad. Sci. U.S.A.* **2004**, *101*, 2673–2677.
(54) Lee, C.; Yang, W.; Parr, R. G. *Phys. Rev. B* **1988**, *37*, 785–789.

radicals. Two main contributions to hfc are usually distinguished in organic radicals, direct and polarization terms.[55] The former is determined by the participation of the s-type valence atomic orbitals in the SOMO and is always positive, while the latter results from the polarization of the s-orbitals (most importantly, of the core orbitals) by the spin density and can be either positive or negative. The contributions can be simply quantified with the use of DFT calculations. If the spin-unrestricted formalism is used, predicted hfc constants include both terms, while in the spin-restricted (RO) approach, the polarization term is neglected. The correlation coefficient and scaling factor for the hfc constants for **60-4-1**$^-$ and **60-6-1**$^-$ predicted at the RO-B3LYP/aug-cc-pCVTZ level are listed in Table 1. From the comparison with the U-B3LYP/aug-cc-pCVTZ values, one can see that direct term constitutes ca. 80%. Thus, despite the fact that the participation of 2s orbitals of fluorine atoms in the SOMO and therefore the spin density are very small (for instance, it cannot be seen in the SOMO plots if typical isovalues of 0.03 are used), we conclude that it is this participation that largely determines the ^{19}F hfc constants in anion radicals of trifluoromethylated fullerenes. The polarization term is smaller but still non-negligible, and in the view of the complexity of the $C_{60}(CF_3)_{2n}^-$ anion radicals, it is crucial that both terms are predicted reliably. For instance, we have found that the poor reliability and large systematic deviations of the 6-311G* basis set are most probably because of the inadequate treatment of the polarization term, because 6-311G* values are close to the hyperfine constants computed at the RO-B3LYP/aug-cc-pCVTZ level (SF = 1.012, R^2 = 0.9862).

Analysis of the Experimental ESR Spectra. ESR Spectrum of 60-4-1$^-$. The anion radical of **60-2-1** did not exhibit hyperfine splitting in the ESR spectrum, and hence **60-4-1**$^-$ is the simplest $C_{60}(CF_3)_{2n}$ compound with well-defined hyperfine structure, and it is also the first member of the radical anions with acenaphthalene-like SOMO (observed when one *nt*-DBIP is present). As mentioned above, the best fit to the experimental spectrum is obtained with two hfc constants, 0.76 G for CF_3 groups in the middle of the ribbon (CF_3-2 and CF_3-3), and 0.21 G for the terminal groups (CF_3-1 and CF_3-4). DFT calculations predict all values to be different, but the order of values is indeed the same as found experimentally; that is, there are two values close to 0.7−0.8 G, and two values that are close to 0.2−0.3 G.

ESR Spectrum of 60-6-1$^-$. The most resolved ESR spectrum among the $C_{60}(CF_3)_{2n}$ derivatives studied was obtained for the **60-6-1**$^-$ (Figure 5), the simplest experimentally available derivative with fulvene LUMO moiety. The hfc values of six CF_3 groups span the 0.16−1.09 G range and are predicted with a high degree of accuracy at the B3LYP/EPR-III or similar levels of theory (Figure 5). The smallest hfc constants are found for the CF_3 groups at the ends of the ribbon (0.163 G for CF_3-1 and 0.244 G for CF_3-6), while the largest values are found for the groups in the middle of the fulvene moiety (1.094 G for CF_3-2 and 0.594 G for CF_3-3) and for the CF_3-5 group (0.919 G) located close to the end of fulvene. In contrast to **60-4-1**$^-$, almost all CF_3 groups in **60-6-1**$^-$ (except for the CF_3-6) are close to carbon atoms with high spin-density. Yet, it appears that this fact is not the only one that determines the magnitude of hfc constants. For instance, the hfc constant of the CF_3-2 group is almost 2 times larger than the value of the CF_3-3 group,

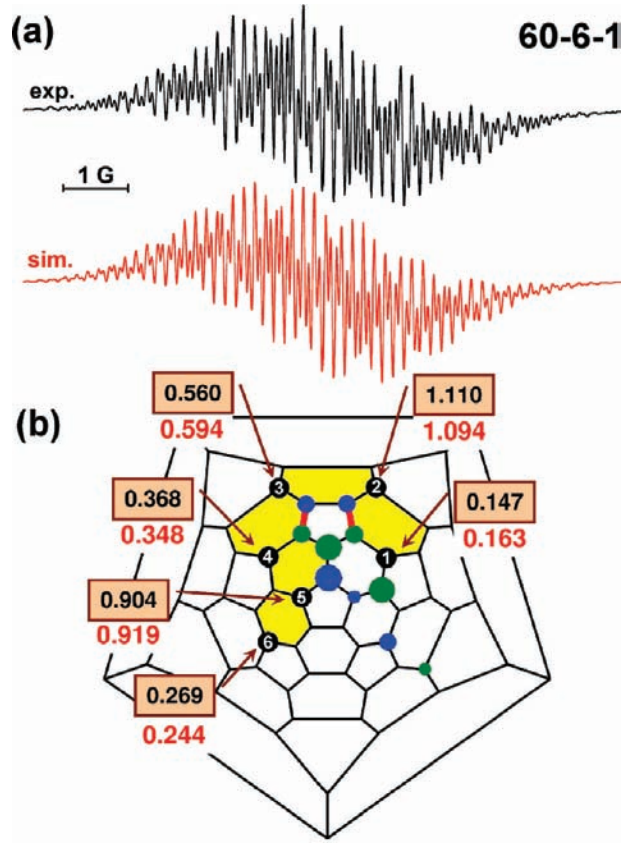

Figure 5. (a) Experimental (black) and simulated (red) ESR spectra of **60-6-1**$^-$; and (b) Schlegel diagram of **60-6-1**$^-$ with DFT-calculated (black numbers in light-brown boxes) and experimental (red numbers) hfc constants. See caption to Figure 1 for further details. Black circles with white numbers denote positions of CF_3 groups and their numbers used in the discussion (note that these are not IUPAC numbers; see ref 6 for the IUPAC numbering in these derivatives), blue and green circles show localization of LUMO, *nt*-DBIPs are highlighted in red, and ribbons of the edge-sharing *meta*- or *para*-$C_6(CF_3)_2$ hexagons are highlighted in yellow.

although both groups have similar neighborhood in terms of the carbon atoms with high spin-density. Likewise, while CF_3-1 has much larger access to the carbon atoms with large spin density, its hfc constant is more than 2 times smaller than that of the CF_3-4 group. Moreover, the hfc constant of the CF_3-6 group, which lacks carbon atoms with a considerable spin density in the neighborhood, is also noticeably larger than that of the CF_3-1 group.

Next, we will show that, although the same CF_3-addition and SOMO pattern is found for some $C_{60}(CF_3)_{10}$ isomers, significantly different hfc constants are predicted and found for the CF_3 groups at the same positions.

ESR Spectrum of 60-10-2$^-$. Among the 10 CF_3 groups of **60-10-2**, six reproduce an addition pattern of **60-6-1**, while four others continue the ribbon of edge-sharing $C_6(CF_3)_2$ hexagons. The complex ESR pattern that can be expected for the **60-10-2**$^-$ anion radical is simplified by the fact that four groups (CF_3-6−CF_3-9) have small hfc constants (<0.03 G) as predicted by DFT and confirmed by simulations (Figure 6a). However, although hfc constants for these groups are very small, they are still larger than the peak-width used in the spectra simulation (0.01 G), and their variation significantly affects the shape of the signal. A very good match to the experimental spectrum can be obtained by simulating the spectrum using the hfc constants shown in Figure 6b. DFT-computed values exhibit

(55) Gerson, F.; Huber, W. *Electron Spin Resonance Spectroscopy of Organic Radicals*; Wiley-VCH Verlag GmbH & Co. KGaA: Weinheim, 2003.

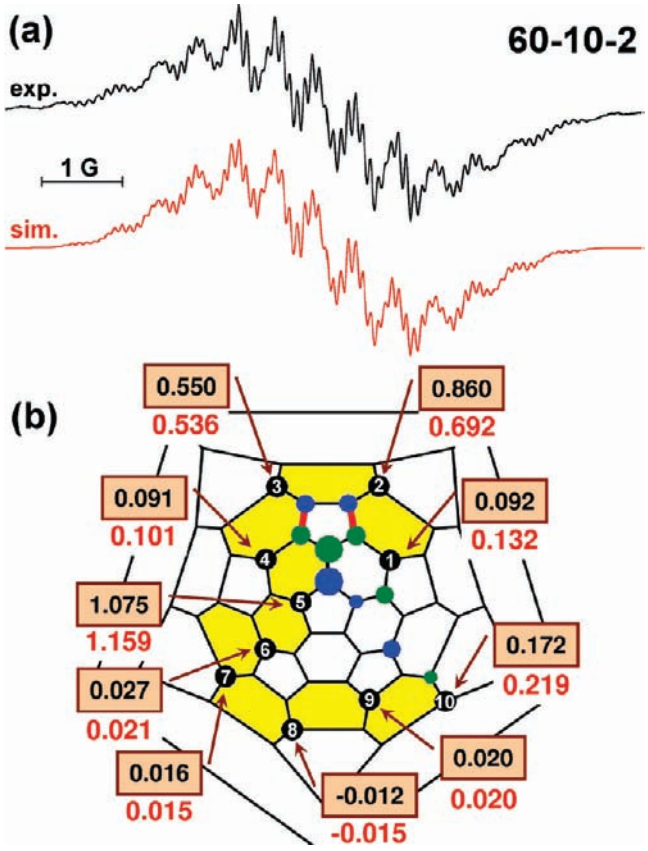

Figure 6. (a) Experimental (black) and simulated (red) ESR spectra of **60-10-2**$^-$; and (b) Schlegel diagram of **60-10-2**$^-$ with DFT-calculated (black numbers in light-brown boxes) and experimental (red numbers) hfc constants. See caption to Figure 5 for further details.

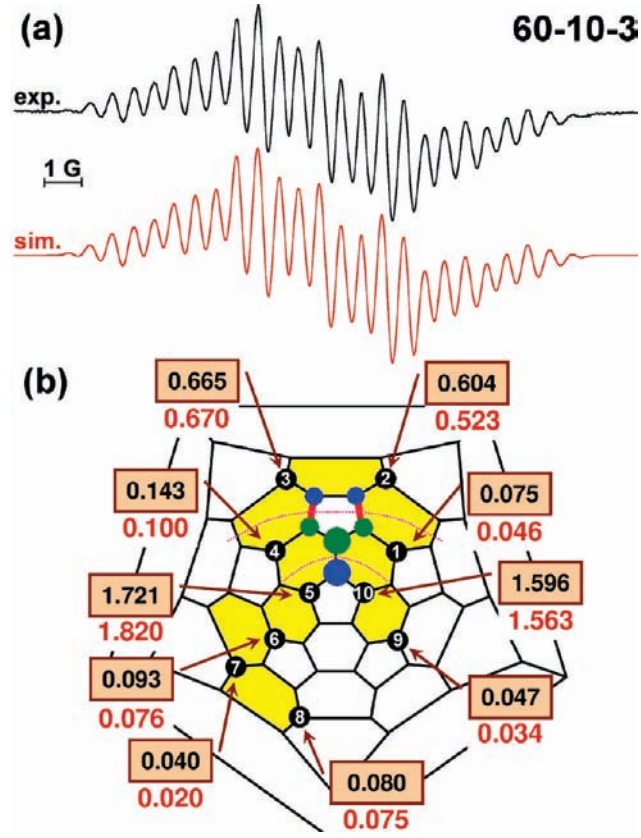

Figure 7. (a) Experimental and simulated ESR spectra of **60-10-3**$^-$; and (b) Schlegel diagram of **60-10-3**$^-$ with DFT-calculated (black numbers in light-brown boxes) and experimental (red) hfc constants. Node surfaces for SOMO are shown by red dotted lines. See caption to Figure 5 for further details.

good agreement with the experimental values except for the hfc constant of the group CF_3-2, which is considerably overestimated by theory (0.860 G vs experimental value of 0.692 G). Despite the close structural similarity and almost identical SOMO pattern, there are considerable differences in hfc constants of CF_3 groups in **60-6-1**$^-$ and **60-10-2**$^-$. First, the CF_3-6 group in **60-10-2**$^-$ has a very small hfc constant ($\sim$0.02 G vs 0.244 G in **60-6-1**$^-$), while the hfc constant comparable to that of CF_3-6 in **60-6-1**$^-$ is found for the group CF_3-10 in **60-10-2**$^-$. Second, the hfc constants for CF_3-1$-$$CF_3$-5 groups in **60-10-2**$^-$ show a larger variation than those in **60-6-1**$^-$: the values of the CF_3-2 and CF_3-4 groups are considerably decreased, while the value of the CF_3-5 group is increased. Nevertheless, the hfc patterns of **60-6-1**$^-$ and **60-10-2**$^-$ seem qualitatively rather similar: the largest hfc constants in both radicals are found for CF_3-2 and CF_3-5 followed by CF_3-3, while the values for CF_3-1 and CF_3-4 are comparably small.

ESR Spectrum of 60-10-3$^-$. The ESR spectrum of **60-10-3**$^-$ was reported by us for the first time in 2006; however, an interpretation was missing up until now. Figure 7a demonstrates an excellent agreement between experimental and simulated spectra, thus allowing a detailed analysis of the hfc constants. Although **60-10-3**$^-$ has a fulvene-like SOMO as **60-6-1**$^-$ and **60-10-2**$^-$, the special feature of this isomer is the fact that the fulvene moiety is isolated from the rest of π-system. This results in the preferable localization of SOMO and spin density on the 6 atoms of the fulvene fragment, while a more extended distribution was found in other radicals with fulvene-like SOMOs. As a result, relatively small hfc constants (less than 0.1 G) are predicted by DFT for those four CF_3 groups that are located far from the fulvene moiety (CF_3-6$-$$CF_3$-9). The values for the CF_3-1$-$$CF_3$-4 groups are comparable to the corresponding values in **60-10-2**$^-$, while hfc constants of the CF_3-5 group are increased by one-half. In addition, a large hfc constant ($\sim$1.6 G) is found for the CF_3-10 group located adjacent to the fulvene moiety.

ESR Spectrum of 60-10-5$^-$. Although **60-10-5**$^-$ has one *nt*-DBIP, and hence its SOMO resembles that of **60-4-1**$^-$, its ESR spectrum (Figure 8) is substantially different from that of **60-4-1**$^-$. According to DFT calculations, hfc constants of four CF_3 groups (CF_3-1, CF_3-6, CF_3-7, and CF_3-8) are less than 0.03 G and will not be considered further. For the rest of the six CF_3 groups, an extended fitting with variation of the initial conditions resulted in two different sets of hfc constants, both providing a good match to the experimental spectrum and noticeable discrepancies from the results of DFT calculations. In one of the sets, the hfc constant for the group CF_3-3 is considerably larger than its DFT counterpart (0.974 G vs 0.795 G), while the value for the group CF_3-5 is smaller than the computed one (0.190 G vs 0.334 G). In another set, the value for the CF_3-5 group is close to the results of DFT calculations. However, the hfc constant of the CF_3-3 group is considerably smaller than predicted by DFT (0.555 G vs 0.795 G), while the value for the CF_3-9 group is noticeably higher than its DFT counterpart (0.544 G vs 0.391 G). The experimental data do not allow us to favor one of the two sets; it is also possible that the reason for the worse agreement of the experiment and theory is in the conformational degrees of freedom (yet we tried and

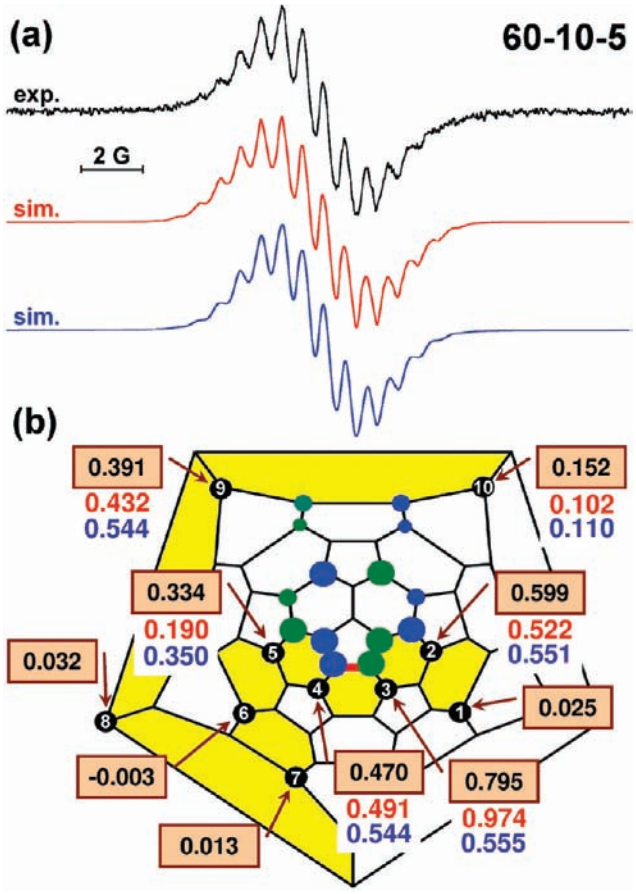

Figure 8. (a) Experimental (black) and simulated (red and blue) ESR spectra of **60-10-5**$^-$; and (b) Schlegel diagram of **60-10-5**$^-$ with DFT-calculated (black numbers in light-brown boxes) and "experimental" (red and blue numbers) hfc constants. The color of the hfc constants in (b) corresponds to the color of the curves in (a). See caption to Figure 5 for further details.

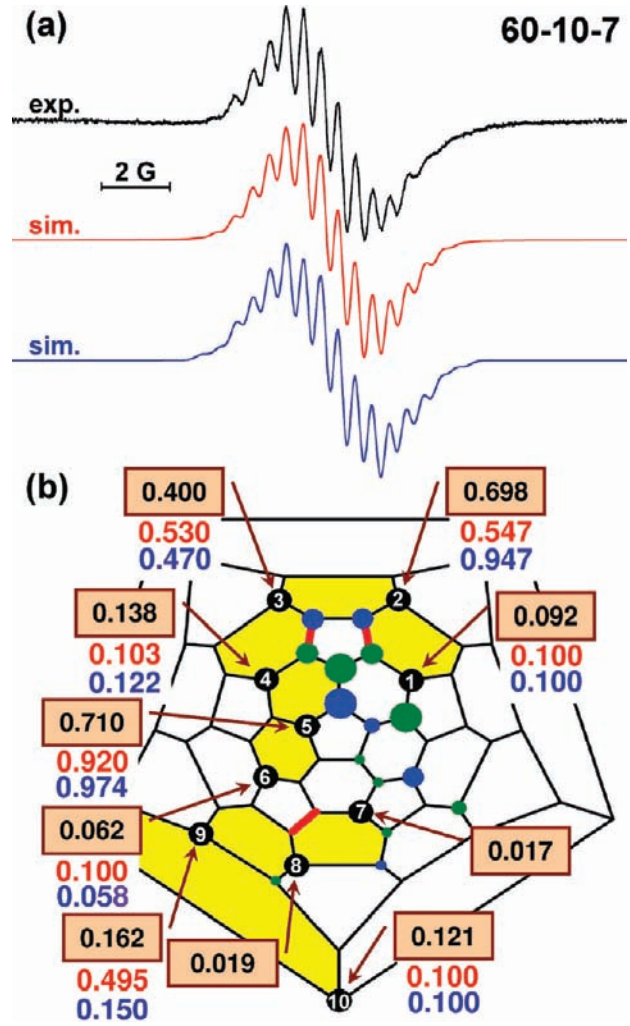

Figure 9. (a) Experimental (black) and simulated (red and blue) ESR spectra of **60-10-7**$^-$; and (b) Schlegel diagram of **60-10-7**$^-$ with DFT-calculated (black numbers in light-brown boxes) and "experimental" (red and blue numbers) hfc constants. The color of the hfc constants in (b) corresponds to the color of the curves in (a). See caption to Figure 5 for further details.

could not find another low energy conformer of **60-10-5**$^-$ with different rotational angles of CF_3 groups). In both sets of values, rather large hfc constants are assigned to the groups CF_3-2 to CF_3-5 and to CF_3-9. In contrast to **60-4-1**$^-$, in which CF_3-1 has an hfc constant of 0.21 G, a very small hfc constant is predicted for CF_3-1 in **60-10-5**$^-$.

ESR Spectrum of 60-10-7$^-$**.** On the basis of the ^{19}F NMR data, DFT calculations of the possible isomers, as well as the electrochemical properties, we have shown that the structure of **60-10-7** includes a fulvene moiety. Moreover, the addition pattern of **60-10-7** and **60-10-2** is different only in the position of two groups. With this respect, it is remarkable that, aside from the broader lines (which therefore does not allow us to observe the very fine structure that can be resolved on the spectrum of **60-10-2**$^-$), the ESR spectra of **60-10-7**$^-$ and **60-10-2**$^-$ exhibit a pronounced similarity. Calculations show that two radicals also exhibit a similarity in the hfc constants for the individual CF_3 groups (that is, large values for the CF_3-2, CF_3-3, and CF_3-5 groups, and relatively small values, on the order of 0.1 G, for the groups CF_3-1 and CF_3-4). Unfortunately, in a more detailed comparison of hfc constants of these two radicals, we have found two sets of hfc constants that fit the experimental data like in the case of **60-10-5**. One of the sets (shown in red in Figure 9) provides a somewhat better match to the experimental spectrum, but the hfc constant for the CF_3-9 group, 0.495 G, is 3 times larger than the value predicted by DFT. In another set, the value of the CF_3-9 group is in good agreement with DFT calculations, while the value for the group CF_3-2 is considerably larger than DFT-predicted one; besides, the fit of the experimental spectrum by this one is not as good as for the first set of hfc constants.

Hfc Constants for Individual F Atoms. The hfc constants of CF_3 groups discussed in the preceding parts of this Article are the averaged values of the three fluorine atoms in each group. Such an averaging is justified by the fast rotation of CF_3 groups, and the results of our analysis indeed prove that interpretation of the spectra can be done on the basis of the assumption of the free rotation. However, it is hardly possible to find any structure−property relationship based on the analysis of the averaged values, and in this section, we analyze the relation between hfc constants for individual fluorine atoms and averaged values for CF_3 on the example of **60-10-3**$^-$ (an excellent agreement between experimental and DFT-computed averaged values for this anion radical ensures reliability of the computed values). The isolated fulvene fragment in **60-10-3**$^-$ has a pseudo C_s symmetry, and hence only three groups can be analyzed in detail. Figure 10 shows a fragment of **60-10-3**$^-$ radical including the fulvene moiety and the surrounding CF_3 groups as well as

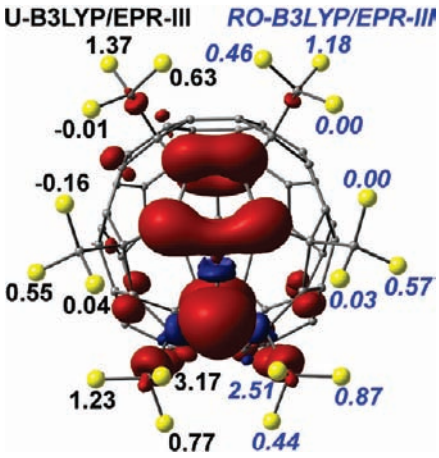

Figure 10. Spin-density in the fulvene-like fragment of **60-10-3**$^-$. Hfc constants of fluorine atoms in the CF_3-3, CF_3-4, and CF_3-5 groups computed at the U-B3LYP/EPR-III and RO-B3LYP/EPR-III levels are shown in black and blue, respectively. The fragment has quasi-C_s symmetry, and the hfc constants of the other three groups (CF_3-10, CF_3-1, and CF_3-2) are similar and not shown here.

the spin-density distribution in this fragment. Hfc constants for fluorine atoms in CF_3-3, CF_3-4, and CF_3-5 computed at the U-B3LYP/EPR-III level are shown in black, while the values for the same atoms but computed at the RO-B3LYP/EPR-III level are shown in italic font and highlighted in blue. Four main features can be summarized as a result of the analysis.

First, the individual hfc constants are substantially different from the averaged values for CF_3 groups.

Second, for relatively large hfc constants, the polarization term is usually positive and can reach 0.66 G (for one of the atoms in the CF_3-5 group).

Third, the smallest hfc constants are found (a) for the fluorine atoms in the CF_3-3 (CF_3-2) and CF_3-4 (CF_3-1) groups sharing the same hexagon, and (b) for atoms from the CF_3-4 (CF_3-1) group sharing a hexagon with the CF_3-5 (CF_3-10) group. To explain the small hfc constants for these fluorine atoms, we have analyzed the spatial distribution of the SOMO in more detail. In addition to the nodal surface coinciding with the surface of the fullerene cage, the orbital has two other nodal surfaces: one of them bisects the fulvene pentagon into two parts with two and three atoms, while another one bisects the double bond radiated from the pentagon (these surfaces are shown in Figure 7 by dotted lines). If one mentally continues these surfaces, they should pass through the hexagons shared by CF_3-3 (CF_3-2) and CF_3-4 (CF_3-1) groups in the first case and by CF_3-4 (CF_3-1) and CF_3-5 (CF_3-10) groups in the second case. Thus, the fluorine atoms that are located close to the nodal surfaces have very small (or even negative) hfc constants, such as the two fluorine atoms in the CF_3-4 (CF_3-1) group and one fluorine atom in the CF_3-3 (CF_3-2) group. Note that, while CF_3-3 (CF_3-2) and CF_3-4 (CF_3-1) groups are staggered with respect to the carbon cage, the CF_3-5 (CF_3-10) group is almost eclipsed. As a result, fluorine atoms of the latter are further from the node surface as compared to the CF_3-4 (CF_3-1) and exhibit larger hfc constants.

Fourth, the largest hfc constant is found for the fluorine atom in the CF_3-5 (CF_3-10) group located at the carbon atom with the largest spin density population; the same atom has the largest positive polarization contribution as well. At the same time, in the other CF_3 groups, the largest hfc constants are found for the fluorine atoms located over pentagons in an *anti*-position to the sp^2-carbon atoms of the fulvene moieties so that the $C(sp^2)-C-C-F$ dihedral angle is close to 180°.

Analogous distribution of hfc constants is found in other radicals. The main sources for differences in the hfc constants are the somewhat different conformations of CF_3 groups and the somewhat different spin populations of carbon atoms.

Vis−NIR Absorption Spectra of $C_{60}(CF_3)_{2n}$ Anions. The use of a second spectroscopic technique in the spectroelectrochemical studies provides complementary information on the electrochemically generated species. Besides, characterization of diamagnetic and, therefore, EPR silent dianions is thus possible with vis−NIR absorption spectroscopy. Figure 11 shows the difference absorption spectra measured during cyclic voltammetry of **60-2-1**, **60-4-1**, and **60-6-1** at the first and second reduction steps. In the charged form, all compounds exhibit new absorption features in the NIR range, which is typical for anions of fullerenes and their derivatives. However, the spectral pattern is different from that of C_{60} and cycloadducts of C_{60} in the anionic states. While the latter are known to exhibit one NIR band at 1080/950 nm (C_{60}^-/C_{60}^{2-})[33] or at ca. 1010 nm (monoanions of cycloadducts),[56] two NIR bands are observed in the spectra **60-2-1**, **60-4-1**, and **60-6-1** in the mono- and dianionc states (note that absorptions of the dianions are more intense). A significant difference in the NIR absorption spectra of the anions was earlier reported for two isomers of $C_{60}(C_6H_5CH_2)_2$ by Kadish et al.[57] While only one NIR band at 1030/905 nm was observed for the anion/dianion of the 1,2-isomer (with benzyl groups attached to the adjacent carbon atoms), two NIR bands at 989/1498 nm (anion) and 903/1294 nm (dianion) were found in the spectra of the 1,4-isomer. The latter is isostructural to **60-2-1** studied in this work, and the spectral features of the anions and dianions exhibit a remarkable similarity (however, absorptions of **60-2-1**$^{-/2-}$ are blue-shifted). It is known that absorption spectra of the fullerene derivatives are very structure sensitive in terms of the addition pattern, but the nature of the addends is relatively unimportant. The same appears to be true for the absorption spectra of the anionic forms. Besides the structural sensitivity of the NIR absorption bands of the fullerene derivatives in the anionic states, these data show that one cannot simply rely on the information known for the C_{60} anions in interpreting the spectra of the fullerene derivatives.

To interpret the experimental data, we have performed TD-DFT calculations of the excitation spectra of the compounds in the charged states. MO levels of the neutral compounds and corresponding monoanions as well as the most intense transitions are schematically shown in Figure 11d. LUMO of C_{60} is 3-fold degenerate, and in the anionic states C_{60} is subject to Jahn−Theller distortion. The intense NIR band of C_{60}^-/C_{60}^{2-} corresponds to the 2-fold degenerate transition from the single-occupied MO to the LUMO+1-derived orbital as shown in Figure 11d. Excitation energy predicted by TD-DFT for this transition is 1054 nm (1.18 eV), which is very close to the experimental value of 1080 nm (1.15 eV). Lowering of the symmetry by addition of two groups (or one cycle), while retaining to a large extent an electronic structure of the fullerene, should result in the splitting of the NIR band of C_{60}^-/C_{60}^{2-}. This was indeed found for the anions of the $C_{60}(CF_3)_{2-6}$ derivatives (Figure 11a−c). At the same time, for the 1,2-derivatives, our calculations demonstrate that only one of the transitions, which is

(56) Sun, Y. P.; Drovetskaya, T.; Bolskar, R. D.; Bau, R.; Boyd, P. D. W.; Reed, C. A. *J. Org. Chem.* **1997**, *62*, 3642–3649.
(57) Kadish, K. M.; Gao, X.; Van Caemelbecke, E.; Suenobu, T.; Fukuzumi, S. *J. Phys. Chem. A* **2000**, *104*, 3878–3883.

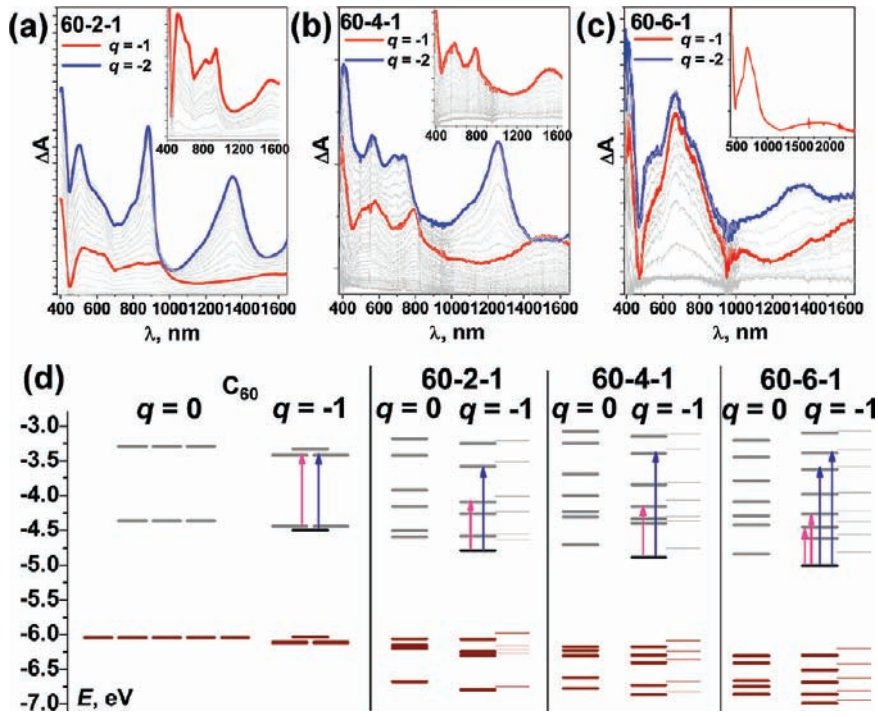

Figure 11. (a−c) Vis−NIR absorption spectra of **60-2-1**, **60-4-1**, and **60-6-1**, respectively, measured during cyclic voltammetry at the first and second reduction steps; the insets show the same for the reduction at the first reduction step of **60-2-1** and **60-4-1**, while the spectrum of the chemically generated anion radical is shown for **60-6-1**; and (d) PBE/Λ01 computed Kohn−Sham MO levels in C_{60}, **60-2-1**, **60-4-1**, and **60-6-1**, and the corresponding anion radicals (for open-shell species, spin-up and spin-down levels are shown separately in thick and thin lines, respectively; however, only spin-up levels are shown for C_{60}^-). Occupied levels are shown in brown, unoccupied levels are shown in gray, and half-occupied level in anions is shown in black. MO energies of the monoanions are ca. 3 eV higher in energy than the corresponding levels of the neutral molecules, and for the sake of comparison they are shifted to match the HOMO energies of the corresponding neutral molecules. The most intense NIR transitions are shown by arrows.

slightly blue-shifted with respect to the C_{60}^- band, shows a high intensity, while the lower-energy component has a very low intensity and cannot be detected in the experimental spectra (see the Supporting Information for more detail on the results of TD-DFT calculations).

For the charged states of **60-2-1**, we have observed two major NIR bands at 942/1550 nm (1.32/0.80 eV) for the monoanion and at 880/1336 nm (1.41/0.93 eV) for the dianion; the lower energy component can be much better seen for the dianion. In good agreement with experimental data, TD-DFT predicts two intense NIR excitations at 978/1562 nm (1.27/0.79 eV) and at 917/1357 nm (1.35/0.91 eV) for the mono- and dianion, respectively. Similar spectroscopic properties are found for **60-4-1**. In the charged states, it exhibits two absorptions at 790/1530 nm (1.57/0.81 eV) and 737/1255 nm (1.68/0.99 eV) for the mono- and dianion, respectively. These bands are very well reproduced by theory, which predicts intense NIR transitions at 801/1480 nm (1.55/0.84 eV) for the monoanion and 757/1267 nm (1.64/0.98 eV) for the dianion. All intense NIR bands are associated with the excitations of the electron from the single-occupied level of the monoanion (and corresponding double-occupied level of the dianion) to the higher energy vacant orbitals.

In the anionic forms of **60-6-1**, we have observed only one broad NIR band centered at 1850 nm (0.67 eV) for the monoanion (because of the limitations of our spectrometer, this band could be observed only for the chemically generated **60-6-1**$^-$ anion; see inset in Figure 11c), which is blue-shifted to 1355 nm (0.91 eV) in the spectrum of the dianion. In these ranges, TD-DFT predicts two NIR transition with comparable intensities at 1500/1989 nm (0.78/0.62 eV) for the monoanion and one intense transition at 1372 nm (0.90 eV) for the dianion. Hence, it is likely that the broad NIR band of the monoanion corresponds to at least two transitions. In addition to the NIR bands, both the mono- and the dianion also exhibit intense features at 670−700 nm. TD-DFT predicts two intense absorptions in this range at 754/878 nm (1.64/1.41 eV) and 766/899 nm (1.62/1.38 eV) for the mono- and dianion, respectively. However, any interpretation of these bands is somewhat ambiguous because of the overlap with the absorption spectrum of the neutral form.

Significant changes in the visible part of the spectrum can be also seen in the charged states of $C_{60}(CF_3)_{2n}$ derivatives, but their interpretation is also rather difficult because of the overlap with the absorptions of the neutral form. Some of the absorptions of the latter are depleted with charging, resulting in the negative peaks that, combined with the increase of the absorptions due to the new peaks of the anions in the same range, can result in false peaks in the difference absorption spectra. In this respect, a discussion of the absorption spectra was mainly focused on the NIR range.

Anions of the derivatives with 8 and 10 CF_3 groups also exhibited NIR bands. However, in most cases, absorptions are limited to wavelengths shorter than 1000 nm. (See the Supporting Information for more details on the spectra of these compounds.)

Conclusions

In this work, we have reported an in-depth study of the charged states of the $C_{60}(CF_3)_{2n}$ derivatives by in situ ESR and vis−NIR spectroelectrochemistry. We have shown that the

complex ESR spectra exhibited by the radical monoanions of trifluoromethylated fullerene can be reliably interpreted by assuming a free rotation of CF_3 groups and applying DFT calculations with subsequent fitting procedure. For a reliable guess for the fitting procedure, it is important that extended or specially tailored basis sets were used for fluorine atoms. In particular, the EPR-III basis set was found to be a reasonable compromise between the accuracy and computational cost. By this method, assignment of the hfc values for individual CF_3 groups was possible for the anion radicals as large as $C_{60}(CF_3)_{10}^-$. To our knowledge, our work is a rare example of detailed interpretation of the CW-ESR spectra of such complex systems; for a combined ESR-ENDOR study of perfluoroalkyl radicals of similar complexity, one can be also referred to the recent work by Okazaki et al.[58]

Strong variations of the hyperfine coupling constants of individual fluorine atoms within one CF_3 group were found and could be explained on the basis of the analysis of the SOMO orbitals. In particular, it was found that small hfc constants are typical for the fluorine atoms located close to the nodal plane of SOMO. By comparing the results of U-B3LYP and RO-B3LYP calculations, we have shown that the direct term constitutes ca. 80% of the hfc constants; besides, in many cases, the polarization term is positive, especially for the atoms with large hfc constants.

Acknowledgment. A.A.P. acknowledges the AvH foundation for financial support and the Computational Center of Moscow State University for a computer time on supercomputer "Chebyshev SKIF-MSU". Technical assistance of U. Nitzsche with local computer resources in IFW is highly appreciated.

Supporting Information Available: NMR spectrum and cyclic voltammogram of **60-10-7**, the list of low-energy isomers of $C_{60}(CF_3)_{10}$ with 6 + 4 addition pattern and their LUMO energies, PBE/TZ2P-optimized Cartesian coordinates of the radical anions and hfc constants computed at the B3LYP level with the EPR-III basis set for fluorine atoms, and vis−NIR absorption spectra of the anions of $C_{60}(CF_3)_8$ and $C_{60}(CF_3)_{10}$. This material is available free of charge via the Internet at http://pubs.acs.org.

JA1043775

(58) Okazaki, M.; Ono, T.; Komaguchi, K.; Ohta, N.; Fukaya, H.; Toriyama, K. *Appl. Magn. Reson.* **2009**, *36*, 89–95.